Long range mutual synchronization of spin Hall nano-oscillators

A. A. Awad[1], P. Dürrenfeld[1], A. Houshang[1], R. K. Dumas[1] & J. Åkerman[1,2]

[1]*Physics Department, University of Gothenburg, 412 96 Gothenburg, Sweden*

[2]*Material Physics, School of ICT, KTH Royal Institute of Technology, Electrum 229, 164 40 Kista, Sweden*

The spin Hall effect[1,2] in a non-magnetic metal with spin-orbit coupling injects transverse spin currents into adjacent magnetic layers, where the resulting spin transfer torque[3–5] can drive spin wave auto-oscillations[6–8]. Such spin Hall nano-oscillators (SHNOs) hold great promise as microwave signal generators and magnonic spin wave injectors. Here we show that SHNOs can also be mutually synchronized with unprecedented efficiency. We demonstrate mutual synchronization of up to nine individual SHNOs, each separated by 300 nm. Through further tailoring of the connection regions we can extend the synchronization range to 4 μm. The mutual synchronization is observed electrically as an increase in the power and coherence of the microwave signal, and confirmed optically using micro-Brillouin Light Scattering microscopy[9,10] as two spin wave regions sharing the same spectral content. Our results enable both highly coherent SHNOs and synchronization based magnonic circuits[11–14] where energy efficient wave computing on the nano-scale may compete directly with CMOS based digital logic.

Spin transfer torque (STT)[3–5] from a spin-polarized current can inject high-amplitude spin

waves[9,10] in magnonic circuits based on so-called nano-contact spin torque oscillators (STNOs)[15–18]. As the wavelength of the injected spin waves is proportional to the size of the nano-contact[19], truly nano-scopic, dipolar-exchange dominated[20] spin waves with a highly directional[21,22] nature can be generated. With the recent advent of the spin Hall effect (SHE)[1,2] substantial STT can also be exerted on a single ferromagnetic layer via a pure transverse spin current generated by a lateral current in an adjacent non-magnetic layer with spin-orbit coupling. The corresponding microwave signal generators, so-called spin Hall nano-oscillators (SHNOs)[6–8,23], exhibit a number of advantages compared to STNOs, such as easier nano-fabrication, reduced current through the magnetic layers, and direct optical access to the magnetodynamically active area.

The high non-linearity[24] of STNOs can promote spin-wave mediated[25] mutual synchronization of multiple nano-contacts over short (sub-micron) distances.[26–28] Whereas SHNOs show a similar non-linearity, and are readily phase-locked to external microwave currents[29], their mutual synchronization remains elusive. A particular limitation of the SHNOs studied to date is the self-localized nature of the dominant mode, which cuts off spin-wave mediated interactions. While nano-constriction SHNOs show signs of a second, possibly propagating, mode[23], they have so far only been studied with their magnetization in the plane[23], where it is known from STNOs that even the inherently propagating mode suffers localization from the magnetic field landscape[21,22].

To mitigate the detrimental effects of spin wave localization, we investigate single and multiple nano-constriction SHNOs in *out-of-plane* fields for the first time. As we increase the applied field angle we find that the generated microwave signal changes dramatically and the optically

observed magnetodynamic region increases in size, consistent with spin waves propagating over longer distances. This is corroborated by the observation that we are able to mutually synchronize as many as nine independent nano-constrictions, each separated from its neighbor by 300 nm. Similarly, in double-constrictions with the same geometry, we demonstrate mutual synchronization for separations up to 1.2 μm. Finally, by reducing the width of the regions connecting the two nano-constrictions we can use the negative damping from the sub-critical current density to extend the synchronization up to separations as large as 4 μm.

Fig.1 summarizes the basic structural and electrical properties of our SHNOs (see methods). Fig.1(a) schematically presents the material stack and device layout, Fig.1(b) shows a scanning electron microscope (SEM) picture of a SHNO with nine nano-constrictions (120 nm wide and separated by 300 nm), and Fig.1(c) displays a spatial map of the lateral current density in the Pt layer, which the transverse spin current entering the NiFe layer is proportional to. As shown in Fig.1(d), the device resistance increases linearly with the number of constrictions; each 120 nm constriction adds 39 Ohm, while the additional series resistance is 70 Ohm. The angular magnetoresistance can be well fitted (inset of Fig.1(d)) by an expression based on anisotropic magnetoresistance with a weak in-plane anisotropy of about 80-130 Oe along the length of the nano-constrictions. Fig.1(e) shows the current dependence of the microwave signal generated by a single nano-constriction in a magnetic field of 0.72 T, tilted 80 degrees out-of-plane, with its in-plane component 66 degrees away from the current direction. At low currents, the signal is weak and exhibits the same red-shifting current dependence as for in-plane fields[23]. At intermediate currents, the frequency shows a clear minimum above which the frequency blue-shifts, the microwave power increases

(Fig.1(f)), while the linewidth shows a non-monotonic behaviour (Fig.1(G)). The local linewidth minimum coincides approximately with df/dI changing sign, consistent with a vanishing oscillator non-linearity in this region.[24]

The more interesting case of double-nano-constrictions is presented in Fig.2, which summarizes our results for five different separations, from 300 nm to 1.2 μm. At low current, each device shows two individual and decoupled signals, with qualitatively the same behavior as in Fig.1(e). The two signals can cross in frequency, as in Fig.2(b)&(e), without interference, frequency pulling or phase locking. The situation changes dramatically at higher currents, where the frequencies blue-shift. For the two closest nano-constrictions, (Fig.2(a)), the two weak signals merge into a much stronger single signal at about 2 mA, indicating their mutual synchronization. This synchronized state remains stable at all higher investigated currents. At a separation of 500 nm, a current of about 2.8 mA is required for mutual synchronization; again, the synchronized state remains stable at all higher currents. At a separation of 700 nm, mutual synchronization first appears at 2.4 mA, is then broken up, until the nano-constrictions again synchronize at about 3 mA. Finally, the nano-constrictions separated by 900 nm and 1.2 μm also show clear regions of mutual synchronization, albeit for a more limited current range. At separations greater than 1.2 μm we were not able to observe synchronization in this geometry. As shown in Fig.2(f)&(g), mutual synchronization is accompanied both by a sharp increase in power and a substantially better linewidth.

To confirm the electrical results through direct optical observation, we mapped out the spatial distribution of the spin wave intensity using scanning micro-Brillouin Light Scattering microscopy

(μ-BLS)[9,10]. Fig.3 shows two rows of spin wave maps on the same device as in Fig.2(d). The upper row corresponds to an un-synchronized state, whereas the bottom row shows similar maps in the mutually synchronized state. Since the spectral resolution of μ-BLS is insufficient to resolve the actual linewidth of the microwave signals and their separation in the un-synchronized state (Fig.3(b)), we do not expect maps of the two states to look very different from each other. This is confirmed in column III in Fig.3(a), where maps for the two states show little qualitative difference. However, as all counts are binned into separate spin wave frequencies we can focus on the high and low ends of the μ-BLS peak, and plot spatial maps of the frequency-selected μ-BLS counts; maps at lower spin wave frequencies are shown in columns I & II, and maps at higher spin wave frequencies in columns IV & V. We then clearly see that while the maps of the mutually synchronized state do not change other than in their overall intensity, the maps of the un-synchronized state change entirely, indicating how the spin waves in the two nano-constrictions have different frequencies. At the lowest mapped frequency there are essentially no counts in the lower nano-constriction, and at the highest mapped frequency there are very few counts in the upper nano-constriction. This is further quantified in Fig.3(d) where we plot the fraction of counts in the upper and lower halves of the maps for both the synchronized and non-synchronized case. Clearly, the relative counts do not change in the synchronized state, implying that their spectral spin wave content in both nano-constrictions is identical.

To investigate whether we can observe mutual synchronization of more than two nano-constrictions, we fabricated SHNOs with multiple nano-constrictions ranging from two to eleven, all separated by 300 nm. The highest number of mutually synchronized nano-constrictions we

have been able to observe is nine (Fig.4), *i.e.* three times more than nano-contacts in STNOs[28]. As in Fig.2, the individual nano-constrictions generate separate microwave signals at low current. As the nano-constrictions pass their minimum frequency, their mutual interactions increase with regions where most, but not all, are mutually synchronized. At a current of 3.86 mA we however observe a single, high-power microwave peak with a very narrow linewidth of about 800 kHz and a peak power of 2700 nV^2/Hz, suggesting that all nano-constrictions have synchronized.

As for STNOs, the mechanism for mutual synchronization of SHNOs is likely spin wave mediated interactions[25] and the observed upper limit of 1.2 μm hence a consequence of spin wave damping in the bridge connecting the two nano-constrictions. If so, it should be possible to further extend the maximum range of mutual synchronization by reducing the spin wave damping in the bridge. This can in principle be achieved through the same spin Hall effect driving the auto-oscillations in the nano-constrictions. By reducing the width of the bridge, and hence the current spread, we should be able to hold the local current density just below the auto-oscillation threshold and greatly extend the distance that spin waves can propagate between the nano-constrictions before being damped out.

Fig.5(a) shows the electrical microwave signal of such a double-SHNO device where two 140 nm nano-constrictions, separated by 4 μm, are connected by a bridge that only opens up about 5 degrees. When a current of 2.2 mA is driven through the device, two individual microwave signals appear. When the current is further increased, the two signals merge, the power increases, and the linewidth improves, all strong indications that the two SHNOs have indeed synchronized

over a distance as long as 4 μm. We investigated two such devices, as well as devices with shorter separations of 3 and 2 μm, which all showed mutual synchronization. Fig.5(b) shows a spatial μ-BLS map of the device in the same field and at a current of 2.4 mA. It is clear from the map that the auto-oscillation regions reside close to the nano-constrictions but inside the connecting bridge. In a device with 4 μm nano-constriction separation, the actual separation of the centers of the two oscillating regions is hence somewhat reduced to about 3.7 μm. If the current is increased, we expect the auto-oscillating regions to further expand towards the center of the connecting bridge as the points where the local current density reaches the auto-oscillation threshold move inwards. Fig.5(c) shows μ-BLS line scans along the x direction of the device and clearly demonstrates that the auto-oscillating regions expand inwards, while their outer boundaries remain static. The approximately linear current dependence of the expansion also reflects the linear profile of the width of the bridge. The long-range nature of the mutual synchronization hence appears to be a combined effect of both reduced spin wave damping and the two auto-oscillation regions approaching each other at high current.

While mutual synchronization is an important step to meet the power and phase noise requirements of commercial applications, our demonstration of robust synchronization over very large distances and for a large number of nano-constrictions, also opens up for additional intriguing possibilities, *e.g.* in spin wave computing.[11–14] Whereas all nano-constrictions in this work were placed on a single line, we expect more complex nano-constriction arrangements to also operate successfully and show synchronization. One may *e.g.* envision spin wave majority gates[12,14] where three or more smaller nano-constrictions are connected to a larger nano-constriction such

that they all operate at the same current density and approximately the same frequency. When driven into mutual synchronization, the phase of the output nano-constriction will then acquire the majority phase value of the inputs.Wave computing can also be used in oscillatory neural networks, and as neural synchronization has been demonstrated to govern associative memory processes[30], SHNO networks with tunable coupling strengths may mimic neurons in the brain.

We have demonstrated robust mutual synchronization of two nano-constriction SHNOs at separations up to 4 μm, and mutual synchronization of up to nine nano-constrictions separated by 300 nm. The synchronized state is characterized by a strong improvement in microwave signal power and coherence. The relative ease of fabrication of strongly synchronized nano-constriction SHNOs will enable the design and fabrication of more complex nano-constriction based architectures where both digital and analog spin wave based computing can be realized.

Methods

Sample fabrication. A bilayer of 6 nm Pt and 5 nm Py ($Ni_{80}Fe_{20}$) was magnetron sputtered in a system with a base pressure lower than 3×10^{-8} Torr at room temperature onto a 20 mm$\times$20 mm piece of sapphire C-plane substrate and *in situ* covered with 5 nm SiO_2 to prevent the permalloy layer from oxidation. The bilayer was then patterned into 4 μm$\times$12 μm rectangles with different bow tie shaped constrictions by e-beam lithography and subsequent argon ion milling using negative e-beam resist as the etching mask. The devices were then covered with an additional 50 nm SiO_2 layer to protect them from oxidation during measurements. A coplanar waveguide provides electrical contacts and is defined by optical lithography, reactive ion etching of the protective SiO_2

layer, sputtering of copper, and lift-off.

Electrical characterisation. All measurements were performed at room temperature. We mounted the sample with a fixed in-plane angle of $\varphi \approx 24^\circ$ on a rotatable sample holder between the poles of an electromagnet with a maximum field of $\approx$2 T. The current bias is applied through a high frequency bias-T and the resulting rf oscillations are amplified using a low-noise amplifier and recorded using a 40 GHz spectrum analyser.

μ-BLS characterisation. The magneto-optical measurements were performed using room temperature micro-focused BLS measurements. Spatially resolved maps of the magnetisation dynamics are obtained by focusing a polarised monochromatic 532 nm single frequency laser (solid state diode-pumped) using a high numerical aperture (NA=0.75) dark-field objective. The probing spot is diffraction limited. The scattered light from the sample surface is then analysed by a high-contrast six pass Tandem Fabry-Perot interferometer TFP-1 (JRS Scientific Instruments). The obtained BLS intensity is proportional to the square of the amplitude of the magnetisation dynamics at the corresponding frequency. The μ-BLS setup is equipped with a spectrum analyser connected to the sample via bias-T to measure the electrical and the optical signals simultaneously.

1. Hirsch, J. E. Spin Hall Effect. *Phys. Rev. Lett.* **83**, 1834–1837 (1999).

2. Kato, Y. K., Myers, R. C., Gossard, A. C. & Awschalom, D. D. Observation of the Spin Hall Effect in Semiconductors. *Science* **306**, 1910–1913 (2004).

3. Slonczewski, J. C. Current-driven excitation of magnetic multilayers. *J. Magn. Magn. Mater.*

159, L1–L7 (1996).

4. Berger, L. Emission of spin waves by a magnetic multilayer traversed by a current. *Phys. Rev. B* **54**, 9353–9358 (1996).

5. Ralph, D. C. & Stiles, M. D. Spin transfer torques. *J. Magn. Magn. Mater.* **320**, 1190–1216 (2008).

6. Demidov, V. E. *et al.* Magnetic nano-oscillator driven by pure spin current. *Nature Mater.* **11**, 1028–1031 (2012).

7. Liu, R. H., Lim, W. L. & Urazhdin, S. Spectral Characteristics of the Microwave Emission by the Spin Hall Nano-Oscillator. *Phys. Rev. Lett.* **110**, 147601 (2013).

8. Duan, Z. *et al.* Nanowire spin torque oscillator driven by spin orbit torques. *Nat. Commun.* **5**, 5616 (2014).

9. Demidov, V. E., Urazhdin, S. & Demokritov, S. O. Direct observation and mapping of spin waves emitted by spin-torque nano-oscillators. *Nature Mater.* **9**, 984–988 (2010).

10. Madami, M. *et al.* Direct observation of a propagating spin wave induced by spin-transfer torque. *Nature Nanotech.* **6**, 635–638 (2011).

11. Khitun, A., Bao, M. & Wang, K. L. Magnonic logic circuits. *J. Phys. D: Appl. Phys.* **43**, 264005 (2010).

12. Khitun, A. & Wang, K. L. Non-volatile magnonic logic circuits engineering. *J. Appl. Phys.* **110**, 034306 (2011).

13. Macià, F., Kent, A. D. & Hoppensteadt, F. C. Spin-wave interference patterns created by spin-torque nano-oscillators for memory and computation. *Nanotechnology* **22**, 095301 (2011).

14. Klingler, S. *et al.* Design of a spin-wave majority gate. *Appl. Phys. Lett.* **105**, 152410 (2014).

15. Tsoi, M. *et al.* Generation and detection of phase-coherent current-driven magnons in magnetic multilayers. *Nature* **406**, 46–48 (2000).

16. Silva, T. J. & Rippard, W. H. Developments in nano-oscillators based upon spin-transfer point-contact devices. *J. Magn. Magn. Mater.* **320**, 1260–1271 (2008).

17. Bonetti, S. & Åkerman, J. Nano-Contact Spin-Torque Oscillators as Magnonic Building Blocks. *Topics in Applied Physics* **125**, 177–187 (2013).

18. Urazhdin, S. *et al.* Nanomagnonic devices based on the spin-transfer torque. *Nature Nanotech.* **9**, 509–513 (2014).

19. Slonczewski, J. Excitation of spin waves by an electric current. *J. Magn. Magn. Mater.* **195**, 261–268 (1999).

20. Kalinikos, B. A. & Slavin, A. N. Theory of dipole-exchange spin wave spectrum for ferromagnetic films with mixed exchange boundary conditions. *J. Phys. C: Solid State Phys.* **19**, 7013–7033 (1986).

21. Hoefer, M., Silva, T. & Stiles, M. Model for a collimated spin-wave beam generated by a single-layer spin torque nanocontact. *Phys. Rev. B* **77**, 144401 (2008).

22. Dumas, R. K. *et al.* Spin-Wave-Mode Coexistence on the Nanoscale: A Consequence of the Oersted-Field-Induced Asymmetric Energy Landscape. *Phys. Rev. Lett.* **110**, 257202 (2013).

23. Demidov, V. E., Urazhdin, S., Zholud, A., Sadovnikov, A. V. & Demokritov, S. O. Nanoconstriction-based spin-Hall nano-oscillator. *Appl. Phys. Lett.* **105**, 172410 (2014).

24. Slavin, A. & Tiberkevich, V. Nonlinear Auto-Oscillator Theory of Microwave Generation by Spin-Polarized Current. *IEEE Trans. Magn.* **45**, 1875–1918 (2009).

25. Pufall, M., Rippard, W., Russek, S., Kaka, S. & Katine, J. Electrical Measurement of Spin-Wave Interactions of Proximate Spin Transfer Nanooscillators. *Phys. Rev. Lett.* **97**, 087206 (2006).

26. Mancoff, F. B., Rizzo, N. D., Engel, B. N. & Tehrani, S. Phase-locking in double-point-contact spin-transfer devices. *Nature* **437**, 393–395 (2005).

27. Kaka, S. *et al.* Mutual phase-locking of microwave spin torque nano-oscillators. *Nature* **437**, 389–92 (2005).

28. Sani, S. *et al.* Mutually synchronized bottom-up multi-nanocontact spin-torque oscillators. *Nat. Commun.* **4**, 2731 (2013).

29. Demidov, V. E. *et al.* Synchronization of spin Hall nano-oscillators to external microwave signals. *Nat. Commun.* **5**, 3179 (2014).

30. Fell, J. & Axmacher, N. The role of phase synchronization in memory processes. *Nat. Rev. Neurosci.* **12**, 105 (2011).

Acknowledgements We thank M. Madami for assistance in building the μ-BLS microscope, and E. Iacocca and M. Dvornik for discussions. This work was supported by the European Research Council (ERC) under the European Community's Seventh Framework Programme (FP/2007-2013)/ERC Grant 307144 "MUSTANG." This work was also supported by the Swedish Research Council (VR), the Swedish Foundation for Strategic Research (SSF), and the Knut and Alice Wallenberg Foundation.

Competing Interests The authors declare that they have no competing financial interests.

Authors contributions A.A. designed the devices. P.D. and A.H. fabricated the devices. A.A., P.D. and A.H. performed all electrical measurements. R.K.D and A.A. built the μ-BLS microscope. A.A. carried out all optical measurements. All authors contributed to the data analysis and co-wrote the manuscript.

Correspondence Correspondence and requests for materials should be addressed to J. Åkerman (email: johan.akerman@physics.gu.se).

Figure 1 **a**, A schematic illustration of the general SHNO layout, showing the patterned Py/Pt bilayer and the field and current directions used throughout the article. **b**, A scanning electron microscopy (SEM) image of a SHNO with nine 120 nm wide nano-constrictions each separated by 300 nm. **c**, Calculated lateral current density in the Pt layer for a total current of I=2 mA. **d**, Measured SHNO resistance (R) and anisotropic magnetoresistance (AMR) vs. number of nano-constrictions. Each nano-constriction adds about 39 Ohm. Inset: angular field scan of the resistance of a SHNO with nine nano-constrictions showing an AMR of 0.5 %. The red line is a fit allowing for a small in-plane uniaxial anisotropy field (129 Oe) along the nano-constrictions. **e** Power spectral density vs. current of a single 120 nm nano-constriction in an applied field of 0.72 T along φ=24°, and θ=80°. **f** Total microwave power vs. current of the signal in **e**. **g** Linewidth for the signal in **e** as extracted from Lorentzian fits.

Figure 2 Power spectral density vs. current of a SHNO with two 120 nm nano-constrictions separated by **a** 300 nm, **b** 500 nm, **c** 700 nm, **d** 900 nm, and **e** 1.2 μm, in an applied field of 7200 Oe along φ=24°, and θ=80°. **f**, Total microwave power vs. current of the signal in **b** showing a sharp increase as the two nano-constrictions synchronize. **g**, Lorentzian linewidth vs. current of the same signals, showing a substantial improvement upon synchronization.

Figure 3 **μ-BLS measurements.** **a**, Columns **I-V** show spatial maps of the μ-BLS counts in the un-synchronized (upper maps) and synchronized (lower maps) state, with

a frequency selection indicated by the coloured regions in the spectra above and below each panel. **b**, The electrically measured microwave signal (red) overlaid on top of the total μ-BLS spectrum in the un-synchronized state, taken at a current of I= 2.6 mA and in a field of 0.553 T along θ=80° and φ=3°. **c**, SEM picture of the SHNO. **d**, Fraction of the counts in the upper (circles) and lower (squares) half of the synchronized (filled symbols) and un-synchronized (hollow symbols) state respectively. **e**, The electrically measured microwave signal (red) and total μ-BLS spectrum in the *synchronized* state, taken at a current of I=3.5 mA and in a field of 0.64T, again along θ=80° and φ=3°.

Figure 4 Power spectral density vs. current of the SHNO in Fig.1, with nine 120 nm wide nano-constrictions each separated by 300 nm, in an applied field of 7200 Oe along φ=24°, and θ=80°. **Inset a**, Power spectral density in a state where two nano-constrictions have synchronized and a number of weaker un-synchronized nano-constrictions can be seen. **Inset b**, Power spectral density in a fully synchronized state at I=3.74 mA, showing a single narrow and powerful peak.

Figure 5 **a** Power spectral density vs. current of two 140 nm nano-constrictions separated by 4 μm in an applied field of 7400 Oe along the φ=26°, and θ=82°. **b** μ-BLS spatial map of the same device in the same field and at an applied current of 2.4 mA. **c** μ-BLS line scans (logarithmic scale) through the center of the device at increasing currents.

Fig.1

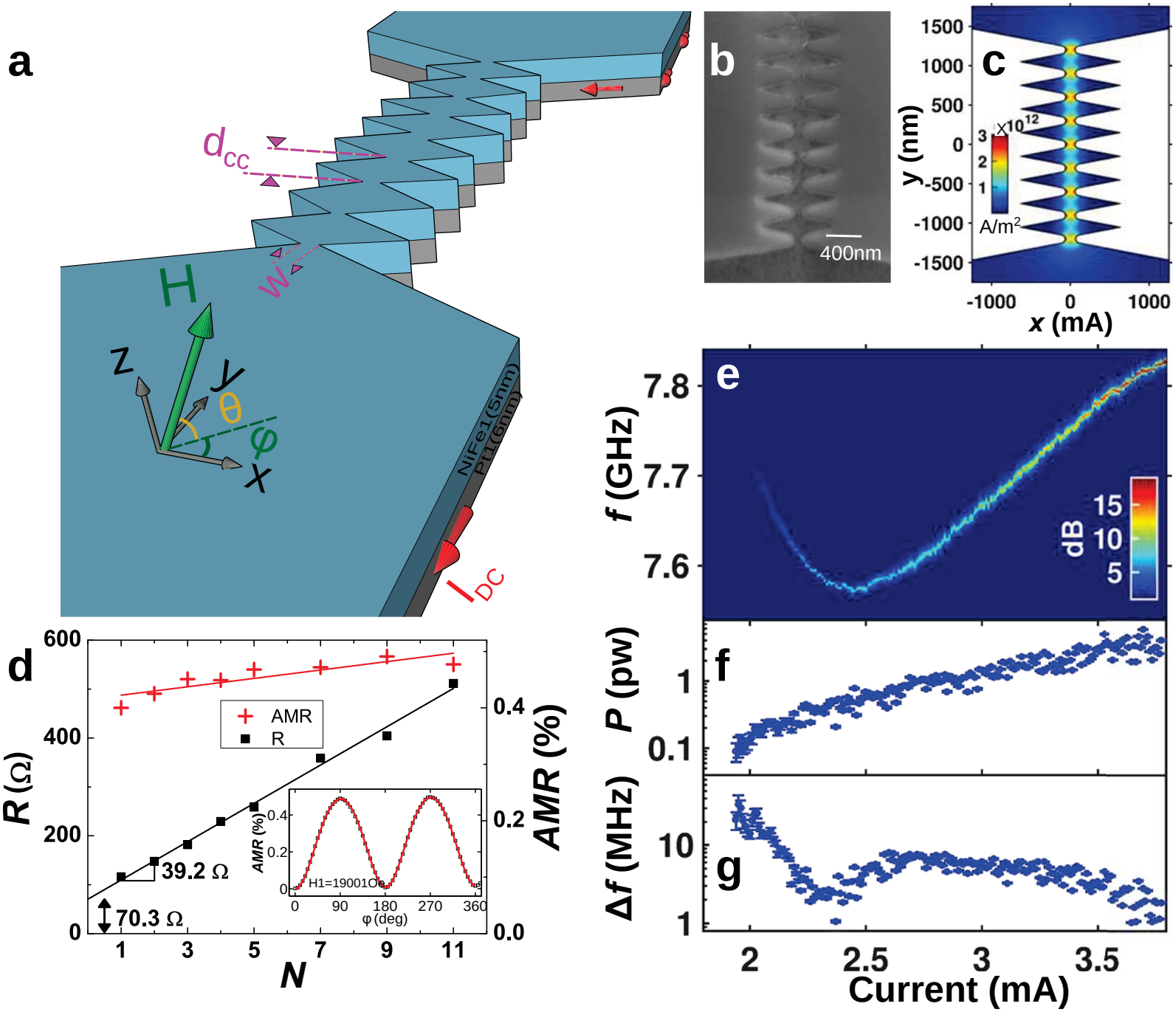
a
d_{cc}
w
H
z
y
θ
φ
x
NiFe1(5nm)
Pt1(6nm)
I_{DC}
b
400nm
c
1500
1000
500
0
-500
-1000
-1500
y (nm)
X10^12
3
2
1
A/m^2
-1000
0
1000
x (mA)
d
600
400
200
0
R (Ω)
AMR
R
39.2 Ω
70.3 Ω
0.4
0.2
0.0
AMR (%)
AMR (%)
0.4
0.2
0
H1=19001Oe
0
90
180
270
360
φ (deg)
1
3
5
7
9
11
N
e
7.8
7.7
7.6
f (GHz)
dB
15
10
5
f
P (pw)
1
0.1
g
Δf (MHz)
10
1
2
2.5
3
3.5
Current (mA)

Fig.2

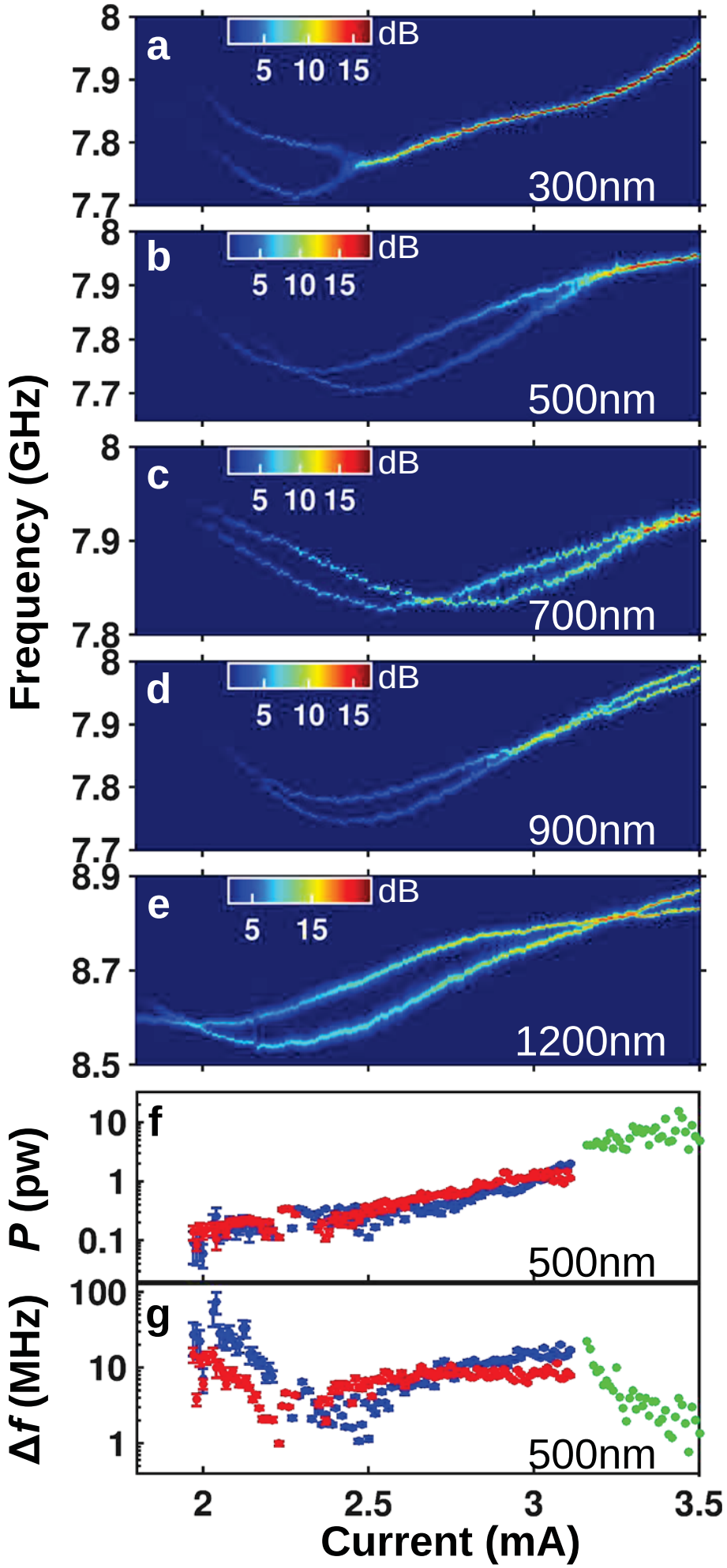
a
b
c
d
e
dB
5 10 15
5 15
300nm
500nm
700nm
900nm
1200nm
Frequency (GHz)
8
7.9
7.8
7.7
8.9
8.7
8.5
f
g
P (pw)
Δf (MHz)
10
1
0.1
100
2
2.5
3
3.5
Current (mA)

Fig.3

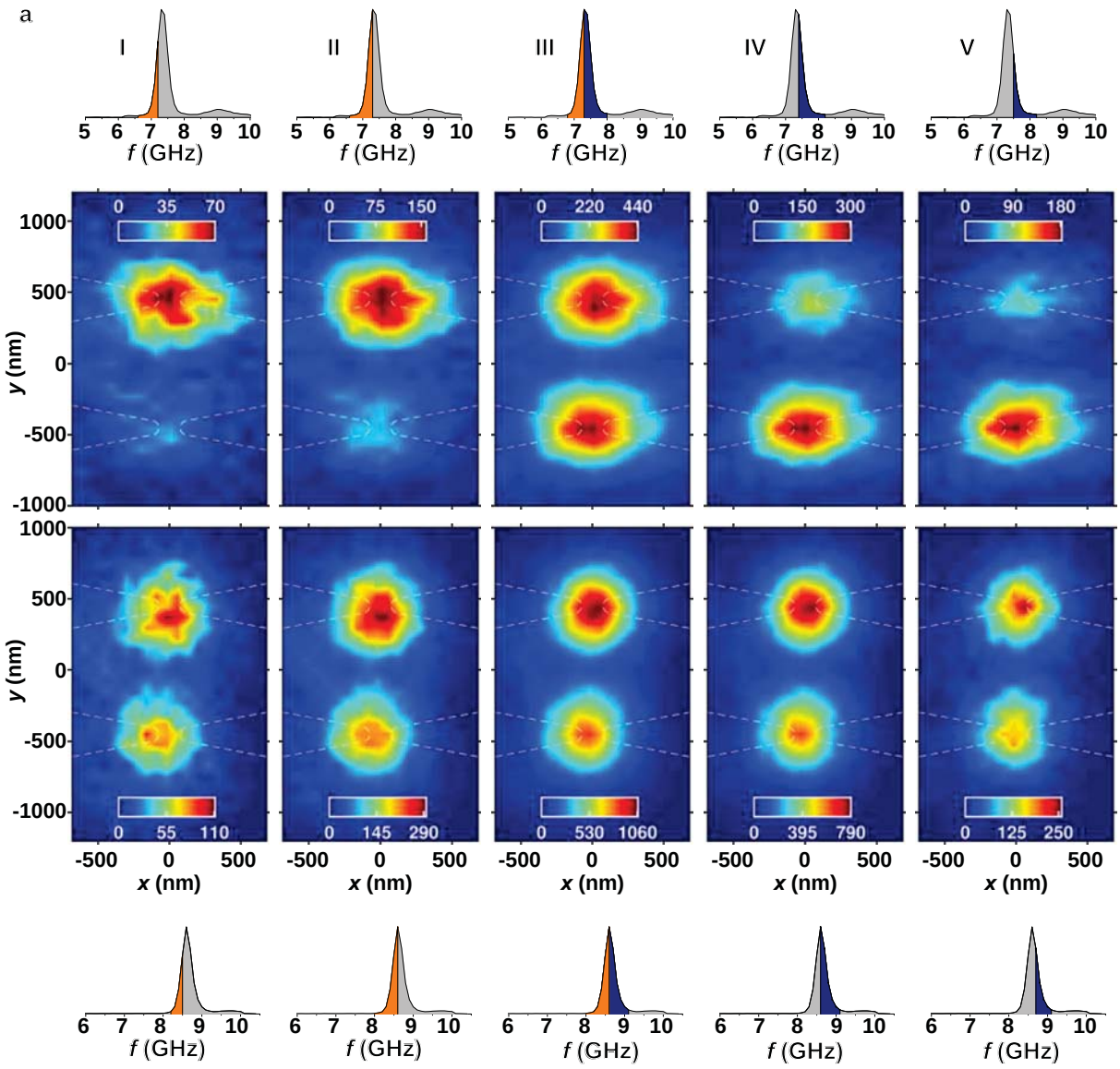
a
I
II
III
IV
V
5 6 7 8 9 10
f (GHz)
0 35 70
0 75 150
0 220 440
0 150 300
0 90 180
0 55 110
0 145 290
0 530 1060
0 395 790
0 125 250
1000
500
0
-500
-1000
y (nm)
-500 0 500
x (nm)
6 7 8 9 10
f (GHz)

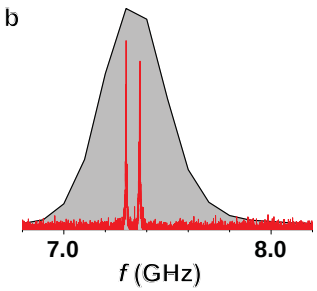
b
7.0
8.0
f (GHz)

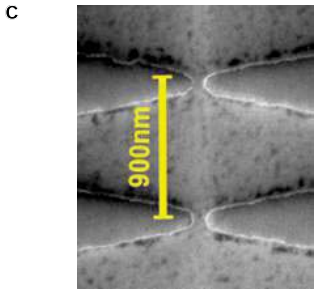
c
900nm

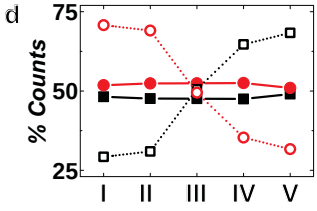
d
% Counts
75
50
25
I II III IV V

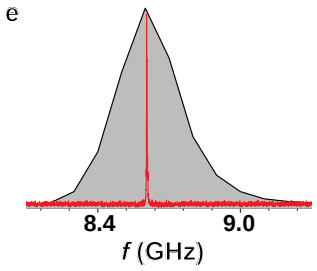
e
8.4
9.0
f (GHz)

Fig.4

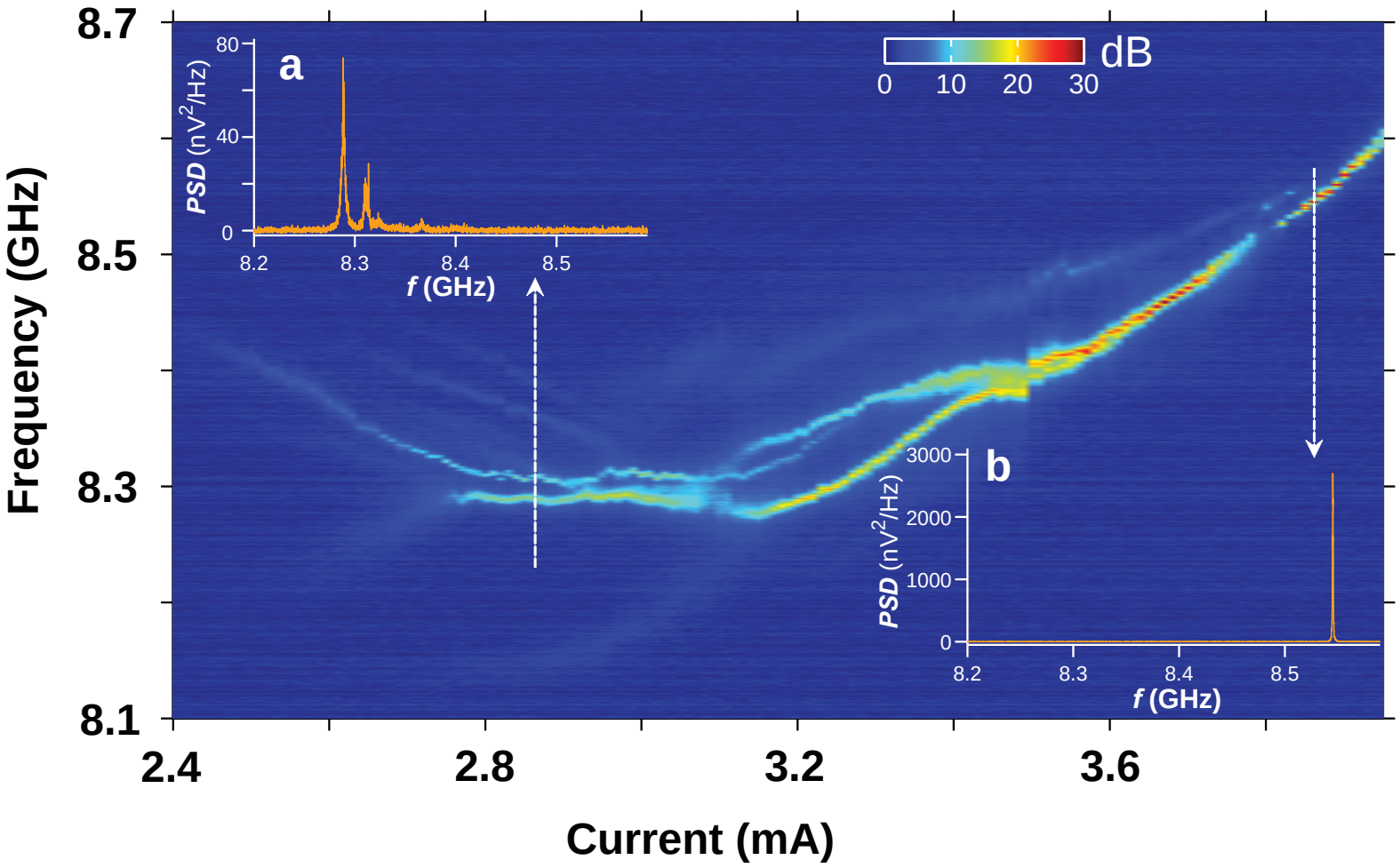
Frequency (GHz)
8.7
8.5
8.3
8.1
2.4
2.8
3.2
3.6
Current (mA)
dB
0
10
20
30
a
PSD (nV²/Hz)
80
40
0
8.2
8.3
8.4
8.5
f (GHz)
b
PSD (nV²/Hz)
3000
2000
1000
0
8.2
8.3
8.4
8.5
f (GHz)

Fig.5

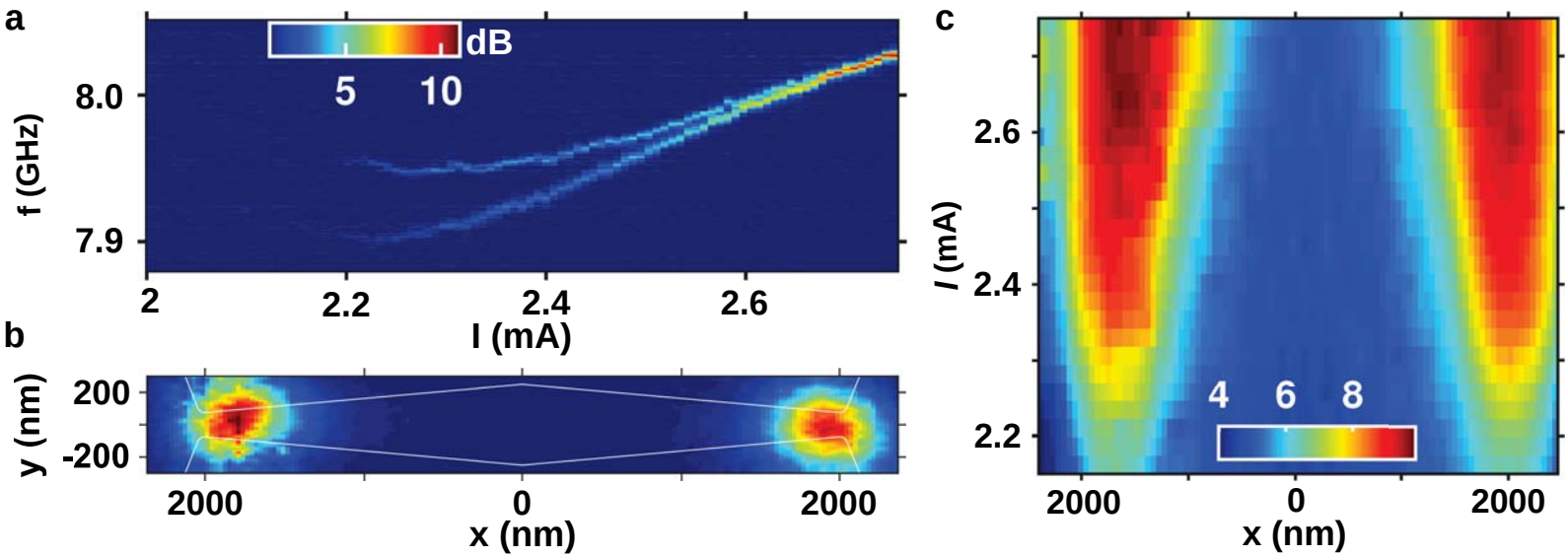
a
dB
5
10
8.0
7.9
f (GHz)
2
2.2
2.4
2.6
I (mA)
b
200
-200
y (nm)
2000
0
2000
x (nm)
c
2.6
2.4
2.2
I (mA)
4
6
8
2000
0
2000
x (nm)